Preparation and characterisation of MCM-41 materials with intra-wall cross-mesopores

Weixing Ming, Jinghong Ma, Yan Wang, R. Li

College of Chemistry and Chemical Technology, Institute of Special Chemicals, Taiyuan University of Technology, Taiyuan 030024, People's Republic of China
E-mail: majinghong@tyut.edu.cn

Published in Micro & Nano Letters; Received on 1st March 2015; Revised on 8th May 2015; Accepted on 8th May 2015

A series of novel mesoporous MCM-41 (Mobil Composition of Matter No. 41) materials has been synthesised using pre-organo-functionalised fumed silica as the silica source. Subsequent X-ray diffraction, nitrogen/argon adsorption and transmission electron microscopy analyses indicated that the additional mesopores formed in silica walls seem to cross the inherent hexagonally arranged channels, affording interconnected structural mesopores. Compared with the conventional MCM-41 material featuring single cylindrical pores, the newly prepared materials have a larger surface area (1450 m^2/g), and their adsorption capacity for n-heptane has been enhanced in the low-pressure region, which presumably would be highly beneficial to the abatement of low-concentration volatile organic compounds.

1. Introduction: MCM-41 (Mobil Composition of Matter No. 41), an ordered siliceous mesoporous material belonging to the M41S family, often possesses a high surface area, large pore volume and narrow mesopore-size distribution. In addition, such material is supposedly derived from a regular hexagonal array of one-dimensional (1D) parallel channels. The pore size of MCM-41 can be effectively modulated within the range of 1.4–10 nm using different template surfactants or synthetic methods; thus, it is not surprising that MCM-41 has found applications in numerous fields. As a matter of fact, such material has been reported to serve as adsorbents, catalysts and catalyst supports, exhibiting excellent physicochemical properties [1–4].

SBA-15 is a mesoporous silica molecular sieve containing uniform hexagonal pores, of which the size distribution is remarkably narrow. Owing to larger pore diameters and thicker framework walls, this material generally possesses a surface area lower than MCM-41. However, the unique property that can truly differentiate SBA-15 from MCM-41 is that it contains secondary porosity, which should originate from micropores and mesopores in the walls as well as connections between parallel mesopores [5]. Consequently, the additional porosity not only facilitates the chemical interaction between adsorbents, but also provides extra transportation channels within the material. It was found that additional pores with a pore size of around 2 nm can be introduced into the porous walls by adding small amounts of poly(vinyl alcohol) into the reaction mixture employed for the synthesis of ordered mesoporous silica, and an increased surface area has been observed [6]. Using polymer or oligomer templates with poly(ethylene oxide) blocks, the 2D hexagonally ordered silica can be readily synthesised, which generally contains connecting pores between mesoporous channels as a common feature of such materials [7].

Herein, we report on the development of a novel method that can efficiently introduce additional mesoporosity into the framework walls of the MCM-41 material. Specifically, using the pre-organo-functionalised fumed silica as the silicon source, and in the absence of polymers, we were able to synthesise a material featuring a high surface area, decent mesoporous connectivity and adequate molecular transporting ability.

2. Experimental: Using trimethylalkylammonium bromide as the surfactant and DTAB (alkyl chain length 12) or CTAB (alkyl chain length 16) as a template, the pre-organo-functionalised fumed silica was employed as the silicon source to synthesise a series of MCM-41 samples. The organo-functionalised fumed silica was prepared from phenylaminopropyl-trimethoxysilane (PHAPTMS, Aldrich) using a procedure described in our previous work [8], with a molar ratio of SiO_2: $67H_2O$: (0.05–0.15) PHAPTMS: $6CH_3OH$. The molar composition of the starting gel for the preparation of MCM-41 samples was SiO_2: 0.25 $C_nH_{2n+1}(CH_3)_3NBr$: 0.2 TMAOH: 40 H_2O. In a typical synthetic process, surfactant and tetramethyl ammonium hydroxide (TMAOH, 25 wt%) were first mixed to obtain a homogeneous solution, followed by slowly adding the organo-functionalised silica to create a uniform, gel-like mixture, which was subsequently heated in an autoclave reactor at 413 K under autogenous pressure for 84 h. After that, the reaction was terminated and the solid product was collected by filtration, followed by washing, drying and calcination at 823 K. On the basis of the carbon chain length of surfactants (C_n) and the amount of organic species incorporated into the silicon, the two series of samples prepared in this work were labelled as MCM-41(C_{12})-1, -2 and MCM-41(C_{16})-3, -4. The content of the organic species in the organo-functionalised silica was 13.8, 19.3, 16.7 and 26.5%, respectively. Reference samples MCM-41(C_n) were synthesised using a similar procedure, except that the silica source employed was fumed silica that does not contain organic functionality.

Samples were characterised by X-ray diffraction (XRD) analysis with a 2θ range from 1.1° to 8° on a Shimadzu XRD-6000. Cell parameters for the measurement of hexagonal symmetry of MCM-41 were obtained by the formula $a_0 = 2 \times 3^{-1/2} d_{100}$. Transmission electron microscopy (TEM) analysis was carried out on a JEOL/JEM-2010 instrument. Thermogravimetric analysis (TGA) was performed on NETZSCH TG 209 F3 from room temperature to 1173K at a heating rate of 10K min^{-1} in air. The adsorption/desorption isotherms of Ar at 87 K and N_2 at 77 K were obtained on a Quantachrome Quadrasorb-SI gas adsorption analyser. The Brunauer–Emmett–Teller (BET) surface area of the samples was determined using the N_2 adsorption data collected within the relative pressure range to ensure a linearity as described by BET equation $p/p_0 = 0.15$, and the total pore volume was determined by a relative pressure of $p/p_0 = 0.90$. The pore size distribution was determined by the non-local density functional theory (NLDFT) method using Ar or N_2 adsorption data [9]. Adsorption isotherms of n-heptane were measured with an intelligent gravimetric analyser (Hiden, IGA-002).

3. Results and discussion: Fig. 1 shows the XRD patterns of the two series of MCM-41 samples prepared in our laboratory. Three diffraction peaks including a main peak and two smaller peaks are evident in the low-angle region. This result indicates that a hexagonally arranged, highly ordered porous structure should be present. Fig. 2 shows the N_2 adsorption/desorption isotherms of MCM-41 samples, which clearly exhibit typical IV isotherm and sharper capillary condensation steps corresponding to ordered porous structures. Therefore, we conclude that this method, in which organo-functionalised silica was utilised as a silicon source, is a viable approach to the synthesis of highly ordered MCM-41 material. As shown in Fig. 1, the position of XRD diffraction peaks (2θ value) for both series has shifted to a higher value area, whereas the silanisation degree of the silica as well as the basal spacing (d_{100}) of samples both decreased markedly. These results are summarised in Table 1. Moreover, it was found that the slopes of the N_2 adsorption isotherm for MCM-41 (C_{12})-1,-2 and MCM-41(C_{16})-3,-4 are steeper than the ones corresponding to MCM-41(C_{12}) and MCM-41(C_{16}), suggesting that a larger mesoporous surface area has been obtained. On the other hand, with the rise of a silanisation degree of silica employed in MCM-41 synthesis, the condensation pressure of MCM-41(C_{12})-1, -2 and MCM-41(C_{16})-3, -4 seems to decline, which indicates that the pore size of MCM-41(C_{12})-1, -2 and MCM-41(C_{16})-3, -4 should be smaller than that of MCM-41(C_{12}) and MCM-41(C_{16}), as confirmed by the XRD analysis. Fig. 2 shows NLDFT pore size distributions of the two series prepared, which also exhibit a similar trend. Specifically, it was found that the average pore sizes for MCM-41(C_{12}) and MCM-41 (C_{12})-1, -2 are 3.18, 2.94 and 2.58 nm, respectively; the average pore sizes for MCM-41(C_{16}) and MCM-41(C_{16})-3, -4 are 3.78, 3.54 and 2.94 nm, respectively. Compared with MCM-41(C_{12}) and MCM-41(C_{16}), the range of pore size distribution for MCM-41(C_{12})-1, -2 and MCM-41(C_{16})-3, -4 has gradually widened to the 'bimodal pore', proving that additional mesoporosity has been successfully introduced into major mesoporous channels. In addition, this result has been unarguably supported by the fact that a much higher surface area was observed in MCM-41(C_{12})-1,-2 and MCM-41(C_{16})-3,-4 samples, as summarised in Table 1.

To further understand the relationship between pore size distribution and micro/mesopore size range, we next collected Ar adsorption/desorption isotherms of MCM-41(C_{12})-2 and MCM-41 (C_{16})-4 within a relative pressure range of 10^{-5}–1.0, as shown in Fig. 2. Notably, similar results have been observed in the isotherm of NLDFT pore size distribution for both Ar and N_2, indicating the presence of secondary mesoporosity. In addition, the pore size distribution calculated from the adsorption kernel on the adsorption branch is in excellent agreement with that obtained from the equilibrium kernel on the desorption branch, suggesting that pore

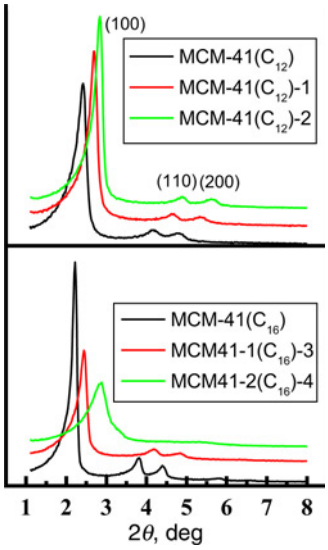

Figure 1 *XRD spectra of MCM-41(C_{12}) and MCM-41(C_{16}) samples*

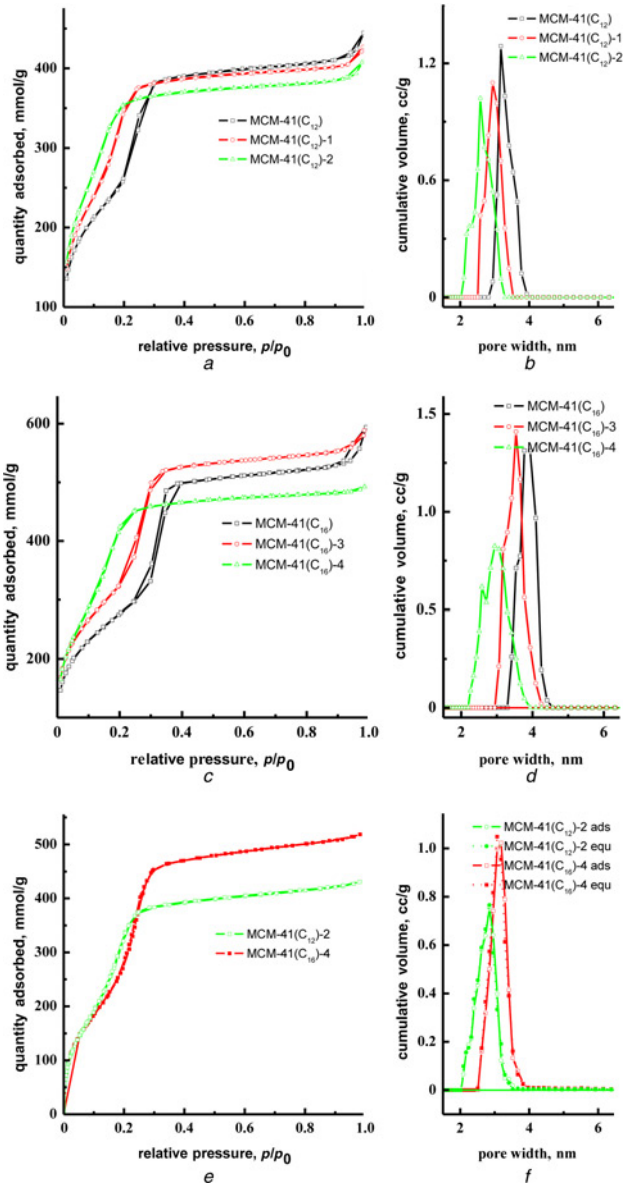

Figure 2 *N_2 and Ar adsorption/desorption isotherms and pore size distribution of MCM-41(C_{12}) and MCM-41(C_{16}) samples*
a–d N_2
e–f Ar

Table 1 Structural parameters of MCM-41 samples

Samples	d_{100}, nm	Unit cell size a_0, nm	S_{BET}, m^2/g	V_{total}, cm^3/g	Pore size, nm
MCM-41(C_{12})	3.751	4.331	917	0.62	3.18
MCM-41 (C_{12})-1	3.327	3.842	1082	0.60	2.94
MCM-41 (C_{12})-2	3.123	3.606	1292	0.59	2.58
MCM-41(C_{16})	4.037	4.662	1010	0.69	3.78
MCM-41(C_{16})-3	3.700	4.272	1171	0.70	3.54
MCM-41(C_{16})-4	3.171	3.662	1452	0.65	2.94

doi: 10.1049/mnl.2015.0078

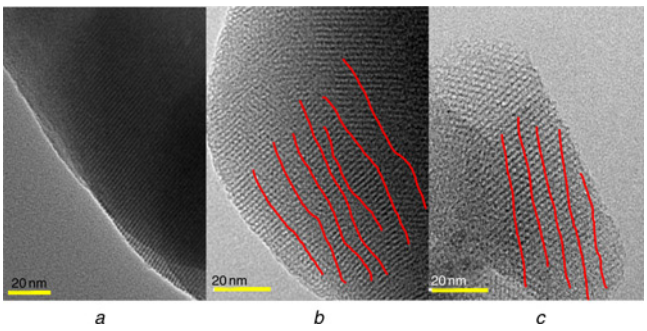

Figure 3 *TEM images*
a MCM-41(C_{12}) sample
b MCM-41(C_{12})-2 sample
c MCM-41(C_{16})-4 sample

blocking should be negligible. On the basis of these results, we believe that a porous network of structural mesopores has been obtained, in which the mesopores across the silica walls seem to be continuous and interconnected [9].

TEM analysis was subsequently conducted to investigate the properties of the porous network structure prepared, including its occurrence and connectivity. The representative TEM images of MCM-41(C_{12}) are displayed in Fig. 3, in which smooth and straight channels are evident in the mesostructures. By contrast, the pore wall of MCM-41(C_{12})-2 samples seems to be mostly disconnected, with some mesotunnels randomly scattering around the wall. Furthermore, the channel walls appear to be partially broken or they tend to connect with each other through lateral connections. Similar pore structure characteristics have been observed in the TEM image of MCM-41(C_{16})-4.

It is well known that the pore size of MCM-41 can be modulated by changing the chain length of surfactant templates. As a matter of fact, it has been found that increasing the surfactant chain length or the pore-to-pore spacing can produce materials with larger pores [1]. Hence, it should not be surprising that the pore size of MCM-41(C_{12}) is smaller than that of MCM-41(C_{16}). Compared with MCM-41(C_{12}) and MCM-41(C_{16}), MCM-41(C_{12})-1, -2 and MCM-41(C_{16})-3, -4 samples exhibit highly extended decrease in pore size and broadening of pore size distribution, which perhaps can be ascribed to the use of organo-functionalised fumed silica. The presence of organic groups in the structure of as-synthesised samples has been confirmed by TGA, as illustrated in Figure 4. Specifically, the TGA curve of MCM-41(C_{16}) shows two weight loss peaks, including the one below 150°C and the one between 150 and 300°C. Theoretically, the former should correspond to the release of physically adsorbed water molecules, while the latter should originate from the combustion of cationic surfactant

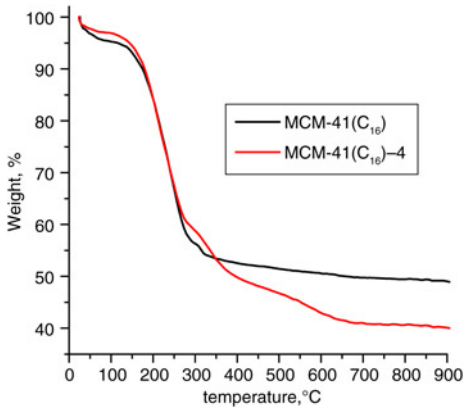

Figure 4 *TGA curves of MCM-41(C_{16}) and MCM-41(C_{16})-4*

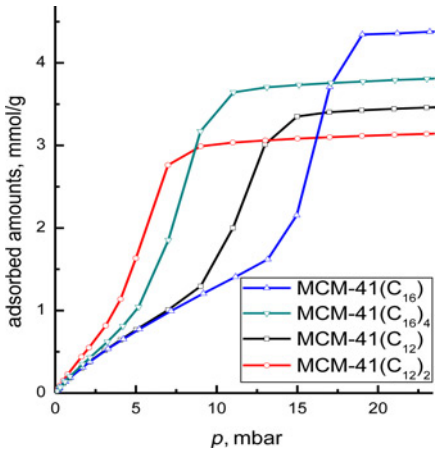

Figure 5 *Adsorption isotherms of n-heptane for MCM-41(C_{12}), MCM-41 (C_{12})$_2$, MCM-41(C_{16}) and MCM-41(C_{16})$_4$*

CTAB incorporated inside the sample. Interestingly, a third weight loss peak in the region of 300–650°C is also evident in the TGA curve of MCM-41(C_{16})-4, which presumably could be attributed to the elimination of organic species covalently bound to the silicon oxide wall of MCM-41 through the newly formed Si–C bond. After calcination, the organic species were mostly removed, resulting in the formation of intra-wall pores. Naturally, the introduction of intra-wall pores can significantly increase the surface area of materials and the concentration of surface silanol groups, thus calcination treatments should lead to larger unit cell contraction and smaller pore size.

The adsorption isotherms of n-hetpane for MCM-41(C_{12}), MCM-41 (C_{12})-2, MCM-41(C_{16}) and MCM-41(C_{16})-4 at 308K are presented in Fig. 5. On the basis of the amount of n-heptane adsorbed under different pressure conditions, we have determined the order of the saturation adsorption capacity as follows: MCM-41(C_{16}) > MCM-41(C_{16})-4 > MCM-41(C_{12}) > MCM-41(C_{12})-2. Notably, the adsorption capacity of MCM-41(C_{12})-2 and MCM-41(C_{16})-4 seems to be much higher than that of MCM-41(C_{12}) and MCM-41(C_{16}) within the low pressure region (<10 mbar), the most common concentration range of volatile organic compounds (VOCs) pollutants. This result indicated that the MCM-41 materials developed in this work have adequately overcome the hurdles involved in practical applications, affording effective adsorbents for low-concentration VOC abatement.

4. Conclusions: In conclusion, novel MCM-41 materials with additional intra-wall mesopores have been readily prepared using functioned organosilane as the silica source. It was found that the structural mesopores in such MCM-41 samples are interconnected with mesopores across the silica walls, affording porous network structures. Compared with conventional cylindrical pore materials, the newly developed mesoporous material possesses a bimodal pore system and higher surface area, thus it has exhibited a remarkable increase in adsorption capacity for n-heptane in the low-pressure region.

5. Acknowledgment: This work was supported by NSFC (grant no. 51272169).

6 References

[1] Kresge C.T., Leonowicz M.E., Roth W.J., Vartuli J.C., Beck J.S. : 'Ordered mesoporous molecular-sieves synthesized by a liquid-crystal template mechanism', *Nature*, 1992, **359**, pp. 710–712
[2] Gibson L.T.: 'Mesosilica materials and organic pollutant adsorption – part: a removal from air', *Chem. Soc. Rev.*, 2014, **43**, pp. 5163–5172
[3] Komura K., Nakano Y., Koketsu M.: 'Mesoporous silica MCM-41 as a highly active, recoverable and reusable catalyst for direct amidation of fatty acids and long-chain amines', *Green. Chem.*, 2011, **13**, pp. 828–831

[4] Wen C.E., Barrow E., Hattrick-Simpers J., Lauterbach J.: 'One-step production of long-chain hydrocarbons from waste-biomass-derived chemicals using bi-functional heterogeneous catalysts', *Phys. Chem. Chem. Phys.*, 2014, **16**, pp. 3047–3054
[5] Kruk M., Jaroniec M., Ko C., Ryoo R.: 'Characterization of the porous structure of SBA-15', *Chem. Mater.*, 2000, **12**, pp. 1961–1968
[6] Zhu J., Kailasam K., Xie X., Schomaecker R., Thomas A.: 'High surface area SBA-15 with enhanced mesopore connectivity by addition of poly(vinylalcohol)', *Chem. Mater.*, 2011, **23**, pp. 2062–2067
[7] Joo S.H., Ryoo R., Kruk M., Jaroniec M.: 'Evidence for general nature of pore connectivity in 2-dimensional hexagonal mesoporous silica prepared using block copolymer templates', *J. Phys. Chem. B*, 2002, **106**, pp. 4640–4646
[8] Xue Z., Ma J., Zhang T., Miao H., Li R.: 'Synthesis of nanosized ZSM-5 zeolite with intracrystalline mesopores', *Mater. Lett.*, 2012, **68**, pp. 1–3
[9] Thommes M.: 'Physical adsorption characterization of nanoporous materials', *Chem. Ing. Tech.*, 2010, **82**, pp. 1059–1073

doi: 10.1049/mnl.2015.0078